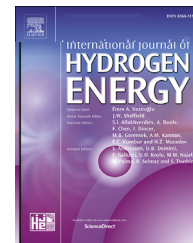


Available online at www.sciencedirect.com

ScienceDirect

journal homepage: www.elsevier.com/locate/hydro

Shaggy-like Ru-clusters decorated core-shell metal-organic framework-derived $\text{CoO}_x@\text{NPC}$ as high-efficiency catalyst for NaBH_4 hydrolysis

Sha ha D^a, Wa Zha g^a, Y i g Ya g^a, Sh i g Zh^a,
Xia fa Ra^b, P a Ya^a, Ta i ja Ta l I i ja^{c,**}, Xi li Ya g^{a,*}

^a Guangxi Key Laboratory of Low Carbon Energy Materials, School of Chemistry and Pharmaceutical Sciences, Guangxi Normal University, Guilin, 541004, China

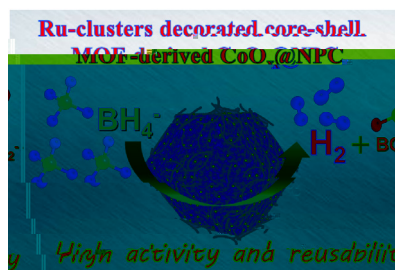
^b School of Resources and Environmental Engineering, Jiangxi University of Science and Technology, Ganzhou, 341000, China

^c Saudi Arabia Basic Industries Corporation (SABIC) at King Abdullah University of Science and Technology (KAUST), Thuwal, 23955-6900, Saudi Arabia

HIGHLIGHTS

- R /CoO @NPC i fab ica ed b a eed-media ed g o h pl p eci e calcina ion.
- The ca al e hibi high ac i i and e abili fo NaBH_4 h d o l i .
- Ca boni ed ZIF-8 and ZIF-67 p o-ide high cond c i i and ich acie i e .
- The pe io pe fo mance a ib- ed o he ne g of Co o ide and R cl e .

GRAPHICAL ABSTRACT



ARTICLE INFO

Article history:

Recei ed 16 A g 2020

Recei ed in e i ed fo m

16 No embe 2020

Accep ed 2 Decembe 2020

A ailable online

Keywords:

Me al-o ganic f ame o k

N-doped po o ca bon

ABSTRACT

Achie ing high ca al ic pe fo mance i h he lo e po ibile amo n of noble me al i c i cal fo an ca al ic applica ion . He in, e epo a con ollable me hod of p epa ing lo R loaded, N-doped po o ca bon embedded i h cobal o ide pecie (R /CoO @NPC) ing co e- hell me al-o ganic f ame o k (MOF) a a empla e. The op imi ed ca al e hibi a high po e fl e able pe fo mance of H_2 p od c ion ho gh odi m bo oh d ide (NaBH_4) h d o l i . The R /CoO @NPC ca al ho a fa H_2 gene a ion a e ($8019.5 \text{ mL min}^{-1} \text{ g}_{\text{ca}}^{-1}$), high no e f eq enc ($1118.6 \text{ mol min}^{-1} \text{ mol}_{\text{R}}^{-1}$), and e - abili . The ca boni ed ZIF-8 co e and he ZIF-67 o e hell p plie a po o ca bon moie ha no onl imp oe he cond c i i and b al o po ide nifo mdi ib ion of he acie i e . The XPS anal i indica e ha he e i a ong elec onic in e ac ion

* Corresponding author.

** Corresponding author.

E-mail add e : iimjan@abic.com (T.T. I imjan), lang@gn.edu.cn (X. Yang).

[h p ://doi.org/10.1016/j.ijhydene.2020.12.011](https://doi.org/10.1016/j.ijhydene.2020.12.011)

0360-3199/© 2020 H d ogen Ene g P blica ion LLC. P bli hed b El e ie L d. All igh e e ed.

Significant effect
NaBH₄ hydrolysis
Hydrogen generation

been compared and reported. The performance can be achieved
to the respective face area and cell area.
© 2020 Hydrogen Energy Publications LLC. Published by Elsevier Ltd. All rights reserved.

Introduction

The growing demand for fossil fuel (e.g., coal, oil and natural gas, etc.) is a significant cause of global warming and led to increased CO₂ emissions [1,2]. The effective development of sustainable energy source and decreasing fossil fuel dependence is the central theme of clean energy research [3]. A sustainable energy carrier, hydrogen is becoming more and more viable due to high energy density and low CO₂ emissions [4]. The main challenge in developing H₂ fuel is the cost and safety issues in the additional H₂ storage in low energy density and complex technical issues. In general, the hydrogen storage methods for both liquid and solid can be divided into physical storage [5], chemical storage [6] and liquid organic hydrogen carrier [7], etc. As a chemical storage approach, the metal hydride (e.g., NaBH₄, LiAlH₄, MgH₂, etc.) has received more and more attention in recent years due to its safety, and adaptability to the mild reaction conditions [8,9]. Among them, sodium borohydride (NaBH₄) has the advantages of high hydrogen density, non-flammability, non-toxicity, and high hydrogen production rate, moderate operating temperature, and stability in alkaline solution, non-oxidative stability [10,11], etc. One of the biggest challenges in using NaBH₄ as the hydrogen storage material is its degradation. However, even after the hydrogen storage material is degraded, it can be regenerated by high-energy ball milling of the hydrolysis product in an ammonia atmosphere [12]. The yield can reach up to 80%, and is recyclable [12]. In addition, some other hydrogen storage materials have been developed with a regeneration efficiency of 60% to 90% [13–15].

However, the presence of hydrolysis of NaBH₄ is a major problem for its efficient and stable use [16,17]. The commonly used catalysts are mainly noble metals, such as Pt/CeO₂-Co₂Ni₂O [18], Pt-Co/carbon nanospheres [19], Pd/PD-ZIF-67 [20], Ag-Ni nanoparticles [21], Pt-Co catalyst [22], Pt/ZIF67 [23], etc. Same as the noble metal catalysts, they are limited by their high cost for industrial application [9]. As a result, many efforts have been devoted to developing Pt-free noble metal catalysts for NaBH₄ hydrolysis to achieve high activity and low cost [14,24,25]. Nevertheless, the efficiency of the Pt-free catalysts is still much lower than that of Pt₃ on carbon. This approach produced a highly efficient and stable catalyst for hydrogen generation from NaBH₄ hydrolysis in alkaline media [28].

The combination of hydrogen, the aim is to improve the catalytic performance of the hydrogen evolution reaction (HER) loading. This goal can be realized by adjusting the properties of the adsorbent and accelerating the reaction rate. Recently, Pan et al. reported a high-performance nano-catalyst based on ZIF-67@ZIF-8 core-shell structure [29]. Based on their work, they claimed that the electrocatalytic performance is the result of the accelerated diffusion kinetics originating from the unique nano-structure [30]. Moreover, the electrocatalytic performance has been demonstrated to be improved by the surface modification and electrocatalytic reaction rate by changing the charge distribution on the carbon surface [31,32]. In light of this, we have designed a novel catalyst of Pt-loaded CoO@NPC using core-shell MOF structure for NaBH₄ hydrolysis. This bifunctional catalyst was prepared in a simple way, namely ZIF-67@ZIF-8 preparation, polymerization, and HER loading. The catalytic performance evaluation has shown that CoO@NPC catalyst has an outstanding H₂ generation rate, low overpotential and durability, far better than the other control catalysts.

Experimental section

Synthesis of ZIF-8 and its degradation catalyst (NPC-8)

All chemical reagents in this work are analytical grade and used without further purification. In a typical synthesis, the polymerization of ZIF-8 was carried out in methanol solution, Zn(NO₃)₂·6H₂O (3 mmol, 30 mL) and 2-methylimidazole (2-MeIm, 12 mmol, 10 mL). Then, the 2-MeIm solution was added to a zinc nitrate solution and aged for 24 h at room temperature. The resulting precipitate was collected by centrifugation, washed three times with methanol and acetone, dried at 70 °C for 12 h. The obtained precipitate was heated at 800 °C in a heating rate of 5 °C min⁻¹ under ammonia atmosphere and kept at 800 °C for 2 h. The collected sample was named as Ni-doped porous carbon (NPC-8).

Synthesis of ZIF-67 and CoO@NPC catalyst (CoO@NPC-67)

First, the solution of Zn(NO₃)₂·6H₂O (1.6 g, 80 mL) and 2-MeIm (3.7 g, 80 mL) was prepared in methanol. Second, the solution of 2-MeIm was quickly poured into the solution of Zn(NO₃)₂·6H₂O and then aged for 24 h at room temperature. The resulting precipitate was collected by centrifugation, washed three times with methanol

and ac m-d ied a 70 °C fo 12 h. Finall , he ob ained p ple po de (ZIF-67) a hea ed o 800 °C i h a hea ing a e of 5 °C min⁻¹ nde A a mo phe e and kep a 800 °C fo 2 h. The e led ample a named a CoO @ni ogen-doped ca bon (CoO @NC-67, incl de Co me al hen = 0).

S he i f ZIF-8@ZIF-67 a d C O @NPC c i e

ZIF-8 (240 mg) a di pe ed in 30 mL of me hanol o fo ma homogeneo pen ion af e 30 min of onica ion. A ock ol ion of Co(NO₃)₂·6H₂O (531 mg, 9 mL) and 2-Melm (2.685 g, 9 mL) a added o he abo e pen ion. Fi e min e la e , he ob ained ol ion a an fe ed o an a ocl e and kep a 100 °C fo 12 h. Af e cooling o oom empe a e , he fo med p eci p a e a cen if ged, a hed i h a la ge amo n of me hanol, and ac m-d ied a 70 °C fo 12 h. The ob ained p ple p eci p a e a e named a ZIF-8@ZIF-67. A a con ol, diffe en mola a io of Co/Zn p e c o e e ed o n he i e a e ie of ZIF-8@ZIF-67. The ZIF-8@ZIF-67 compo i e a hen hea ed o 800 °C i h a hea ing a e of 5 °C min⁻¹ nde A a mo phe e and kep a 800 °C fo 2 h. The e led ample a nomina ed a CoO @ni ogen-doped po o ca bon (CoO @NPC). The con en of C and N in he op imi ed ma e ial a anal ed b an elemen anal e (Table S1), hile Co and Zn e e mea ed b ICP-AES (Table S2).

S he i f R /C O @NPC c i e

T picall , 30 mg CoO @NPC and diffe en ma e of R Cl₃·3H₂O e e l a onicall di pe ed in o 20 mL H₂O o fo ma homogeneo pen ion. Af e con in o i ing fo 5 h, 2 mL of 0.6 M NaBH₄ ol ion a added d op i e in o he abo e mi e. Thi min e la e , he e led black p eci p a e a collec ed b cen if ga ion, a hed h ee ime i h ab ndan a e , and nall f ee d ied a 70 °C fo 12 h o ob ain he nal p od c of R /CoO @NPC. The ICP-AES e e l ho ha he ma pe cen age of R in he compo i e ange f om 1.69 % o 3.38 %, and he R ma pe cen age of 2.73 % ha he be ca al ic pe fo mance.

A a compa ion, a ma pe cen age of 2.72 % R a applied o n he i e all o he con ol ca al . No abl , all he n he ic p o ce e e e a de c ibed abo e be ide ha he ma of he R Cl₃·3H₂O a ed a 8.0 mg, and he ppo a eplaced i h NPC-8, CoO @NC-67, and XC-72 ca bon black, e p eci el . The ob ained ca al e e nomina ed a R /NPC-8, R /CoO @NC-67, and R /CB, e p eci el .

Ca l cha ac e i a i

The c al c e of ca al a anal ed b X- a po de diff ac ion (XRD, Rigak D/Ma 2500 V/PC) i h a eep peed fo 2.0° min⁻¹. The mo phologie and mic o c e of he ca al e e cha ac e i ed b canning elec on mic o cope (SEM, FEI Q an a 200 FEG) and an - mi ion elec on mic o cope (TEM, JEM-2100F). The X- a pho elec on pec ome e (XPS, JPS-9010 Mg K α) a ed o anal e he chemical a e of diffe en elemen . The p eci fic face a ea of he a -p epa ed p od c a mea ed on a

Q an ach ome A o o b AS-1 in men . The ac al load- ing of a io me al in he ca al e e checked b ind ci el co pled pla ma a omic emi ion pec o cop (ICP-AES, IRIS In epid II XSP).

Ca l ic h d l i f H₂ g e e a i

The ca al ic ac i i , c cle abili and ac i a ion ene g of he ca al ic ma e ial e e ob ained b he follo ing me hod . Fi , 50 mL of 150 mM NaBH₄ (con aining 0.4 % NaOH) a added o a h ee-necked ond bo om a k (100 mL) and con in o l i ed in a a e ba ha 25 °C fo 0.5 h n il he connec ed elec onic balance abili ed o e o. Then, 10 mg of he ca al a added o he abo e ol ion a 25 °C nde con in o i ing. The gene a ed H₂ a e al- a ed b d ainage me hod, he e he o e o ed a e a collec ed d ing he ca al ic H₂ p od c ion p o ce and he q ali of he a e a eco ded in eal- ime ia a comp e- connec ed elec onic balance. The h d ogen gene a ion a e (HGR) and no e f eq enc (TOF) can be ob ained b con- e ing he q ali of he d ainage a e o e ime (ee p- plemen a info ma ion) [33,34]. To e he ca al ' e abili , e mea ed he ca al ic pe fo mance e ime a 25 °C. Af e each e abili e , e cen if ged he ca al , d ied i nde ac m a oom empe a e , and ob- ained he ca al ' eigh . All e pe imen e e epea ed h ee ime o en e eliable e l . The ac i a ion ene g of he de igned ca al a e al a ed in he ame de ice in he empe a e ange of 298–318 K.

Results and discussion

S he ic a e g a al i

The chema ic diag am of he p epa a ion me hod of po o R /CoO @NPC compo i e i ho n in Scheme 1. S ep 1: he ZIF-8 a n he i ed b a con en ional manne , in hich a mi e of inc ni a e and 2-Melm in me hanol a aged a oom empe a e fo 24 h [35]. S ep 2: he ZIF-67 a go n on o he ZIF-8 face o fo m ZIF-67@ZIF-8 compo i e h o gh he h d o he mal me hod a 100 °C fo 24 h [30,36]. S ep 3: he ZIF-8@ZIF-67 compo i e a placed in a ce amic boa and ca boni ed a 800 °C o p epa e he CoO @NPC compo i e. S ep 4: he R cl e loading p o ce a accompli hed h o gh di ec chemical ed c ion of R³⁺ ing NaBH₄ ol ion. The ac al R loading e e de e mined b ICP-AES and he co e ponding e l e e ed o calc la e he HGR and TOF al e (Table S3). The e of he con ol e e p epa ed in he imila manne . Mo eo e , a de ailed in e iga ion of he p ol i p o ce of each in e media e ing he mog a ime ic (TG) anal i combined i h ma pec ome (MS) gi e a e fl in igh of he p ol i mechani m (Fig. S1).

C alli i , ic c e a d i a al i

Scanning elec on mic o cop (SEM) ho ed ha he a - p epa ed ZIF-8 and ZIF-67 had a imila pol hed al mo pholog i h an a e age pa icl e i e of 400 nm (Fig .



Scheme 1 – Schematic diagram of the synthesis of Ru/CoO_x@NPC composite.

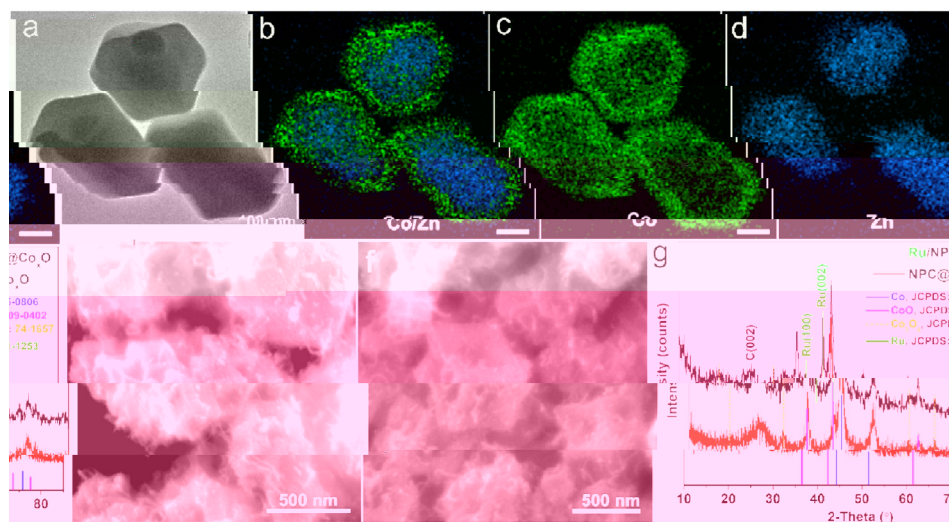


Fig. 1 – (a) TEM image of ZIF-8@ZIF-67 and (b–d) the corresponding elemental mappings of Zn and Co. SEM images of (e) CoO_x@NPC and (f) Ru/CoO_x@NPC composites. (g) XRD patterns of Ru/CoO_x@NPC and CoO_x@NPC.

S2a–b). The ZIF-67@ZIF-8 is about 500 nm in particle size (Fig. S2c), giving a good 100 nm ZIF-67 grown on the ZIF-8. As shown in Fig. 1a, an electron microscopy (TEM) image shows that ZIF-8@ZIF-67 exhibits a clear edge and well-defined polyhedral shape, and the corresponding elemental distribution mapping further clearly demonstrates the existence of the core-shell structure (Fig. 1b–d). Upon calcination at 800 °C for 2 h in air atmosphere, the polyhedral morphology of ZIF-8@ZIF-67 partially inherited the CoO@NPC (Fig. 1e). Interestingly, although the large number of carbon nanobubbles penetrate through the surface of the collapsed polyhedron, and the face-to-face distribution of the main particles is maintained. After chemical reduction of the RuCl₃, it did not observe any noticeable change in the morphology, indicating that the deposition of RuCl₃ on the surface of CoO@NPC does not affect the overall morphology of CoO@NPC (Fig. 1f).

The X-ray diffraction (XRD) patterns of different calcination temperatures and RuCl₃ decomposition temperatures are plotted in detail in Fig. S3. Upon calcination at 800 °C in

air atmosphere (Fig. 1g), the resulting CoO@NPC mainly exhibits the diffraction peaks belonging to the Co species such as Co (JCPDS: 15–0806), CoO (JCPDS: 09–0402), and Co₃O₄ (JCPDS: 74–1657) [20,37]. After chemical deposition of RuCl₃, there are two additional diffraction peaks appeared at 38.6° and 42.4°, which are consistent with the characteristic peaks of the hexagonal structure of metallic Ru (JCPDS: 01–1253) [38]. Moreover, X-ray diffraction (XRD) patterns of ZIF-8, ZIF-67 and core-shell ZIF-8@ZIF-67 are compared in Fig. S4a, and Raman spectra are adopted to investigate the effect of calcination temperature and pyrolysis temperature on the carbon content (Fig. S4b–c).

To further examine the microscopic features of Ru/CoO@NPC composite, we performed a detailed TEM study. Most of the black clusters (probably Co or Ru) are randomly distributed throughout the composite and some of which are aggregated into a bigger particle (Fig. 2a). The high-resolution TEM image clearly shows the lattice spacing of 0.18 nm and 0.20 nm, and the corresponding (111) and (200)

plane of metallic Co (Fig. 2b) [39], respectively. Meanwhile, the lattice fringe spacing of 0.21 nm is assigned to the (200) crystal plane of CoO [40], a lattice spacing of 0.34 nm is corresponding to the (002) crystal plane of graphitic carbon, and the other lattice spacing of 0.23 nm belongs to the (100) crystal plane [41]. Furthermore, the HAADF-STEM and corresponding elemental mapping indicate the presence of Ru, Co, Zn, C, N and O as evidenced by the high-resolution HRTEM image of Ru/CoO@NPC composite (Fig. 2c). Notably, since the particle size of Ru is small, it can hardly distinguish the Ru particle. Notably, the morphology of Ru particle is in line with the feature of the loading of Ru species in the composite.

The N_2 adsorption/desorption isotherm at 77 K of Ru/CoO@NPC composite is shown in Fig. 2d. The BET surface area and pore volume of Ru/CoO@NPC composite are 325.0 $m^2 g^{-1}$ and 0.206 $cm^3 g^{-1}$. The isotherm shows a typical hysteresis loop of type IV (P/P₀ < 0.02), indicating the presence of a mesoporous structure. Notably, the pore size distribution is mainly originated from the collapse of the composite [42]. Moreover, the pore size distribution of the composite is in the range of 0.73–2.7 nm from the Barrett-Johnson-Halenda (BJH) analysis, indicating the micropore and mesopore porous structure. The high porosity, pore volume, and facile diffusion of O_2 and the element of gas, the effective improvement of catalytic performance.

XPS analysis

The composition and chemical state of Ru/CoO@NPC and CoO@NPC were studied by X-ray photoelectron spectroscopy (XPS). As shown in Fig. S5a, the elements of C, N, O, and Co are detected in both samples by XPS respectively. The high-resolution XPS spectra of C 1s + Ru 3d region (Fig. 3a) are deconvoluted into C=C (284.0 eV), C-C (284.8 eV) and C-O (286.1 eV) and deconvoluted into Ru 3d_{5/2} and Ru 3d_{3/2} (Unconvoluted) [45]. Fig. 3b shows the high-resolution Co 2p spectra of Ru/CoO@NPC and CoO@NPC, where the Co 2p_{3/2} region of Ru/CoO@NPC is deconvoluted into three peaks at 778.5, 780.6 and 784.6 eV, corresponding to metallic Co, Co²⁺ and a small peak, respectively. Compared with CoO@NPC, the Co²⁺ species in Ru/CoO@NPC is more abundant (0.93 eV), which may be due to the binding energy difference of Co 2p_{1/2} of Co²⁺ and Co³⁺ (1.2 eV) [46], indicating a stronger interaction between Ru and Co species [47]. Notably, the peak ratio of Co²⁺/Co is increased from 7.6 to 15.2 after the Ru loading on the CoO@NPC surface, which could be due to the oxidation of the surface of CoO@NPC. Moreover, the high-resolution O 1s spectra of the samples are also analyzed (Fig. 3c). The deconvoluted peaks of signal at 529.5, 530.8 and 532.1 eV are assigned to metal oxide, oxygen vacancy and adsorbed H₂O, respectively [48]. As shown in Fig. 3c, the oxygen vacancy is increased from 42.6% to 67.9% after Ru loading. Meanwhile, it is found that a high proportion of oxygen vacancy is due to the fast electron transfer, and the adsorption characteristics and mechanism [49]. Furthermore, it

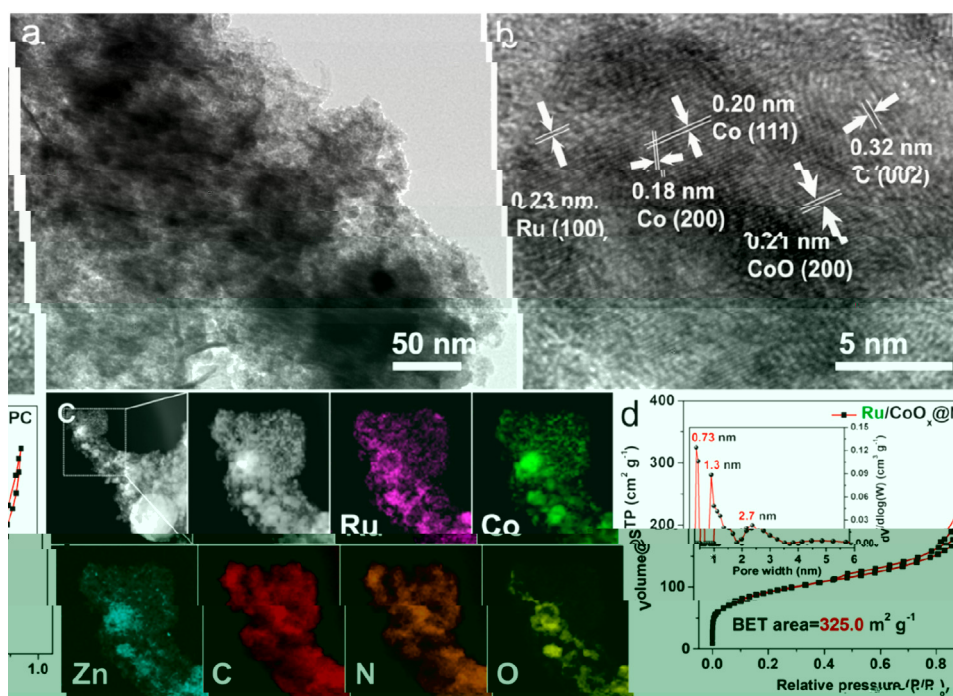


Fig. 2 – (a) TEM and (b) high-resolution TEM images of Ru/CoO_x@NPC. (c) HAADF-STEM image of Ru/CoO_x@NPC, and the corresponding element mappings of Ru, Co, Zn, C, N and O. (d) N_2 adsorption–desorption isotherms with pore-size distributions by the BJH method of Ru/CoO_x@NPC.

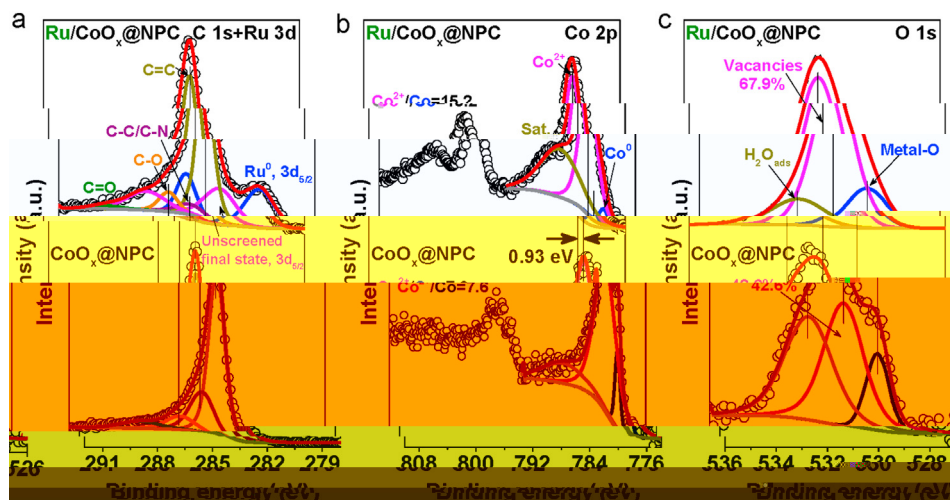


Fig. 3 – High-resolution XPS spectra of (a) C 1s + Ru 3d, (b) Co 2p and (c) O 1s regions from Ru/CoO_x@NPC and CoO_x@NPC.

hold be pointed out that the high-resolution N 1s spectra did not change much before and after the loading of Ru (Fig. S5b–c), further demonstrating that the loading process of Ru does not disturb the composition of the material [50].

Catalytic durability

The catalytic H₂ production from NaBH₄ hydrolysis is performed in an alkaline NaOH solution at 25 °C. The chemical illustration of the experimental setup is shown in Fig. S6. The amount of the generated H₂ is calculated according to the volume of the azeotropically displaced H₂. The eff-

iciency of NaBH₄ is carried out in 150 mM NaBH₄ + 0.4 % NaOH solution, and almost no hydrogen evolution is detected (Fig. S7). As shown in Fig. 4a, we explored the effect of the carbonyl ion impregnation of Ru/CoO_x@NPC on catalytic performance. The higher annealing temperature changes the catalyst's crystallinity, which improves catalytic performance; meanwhile, it also decreases the catalyst's porosity. Therefore, the optimal point is expected. The results show that the optimized Ru/CoO_x@NPC catalyst prepared by carbonyl impregnation at 800 °C has the highest turnover frequency (TOF) of 1118.6 mol_{H₂} mol_R⁻¹ min⁻¹ among the catalysts (Fig. 4b). This is one of the highest reported values of Ru

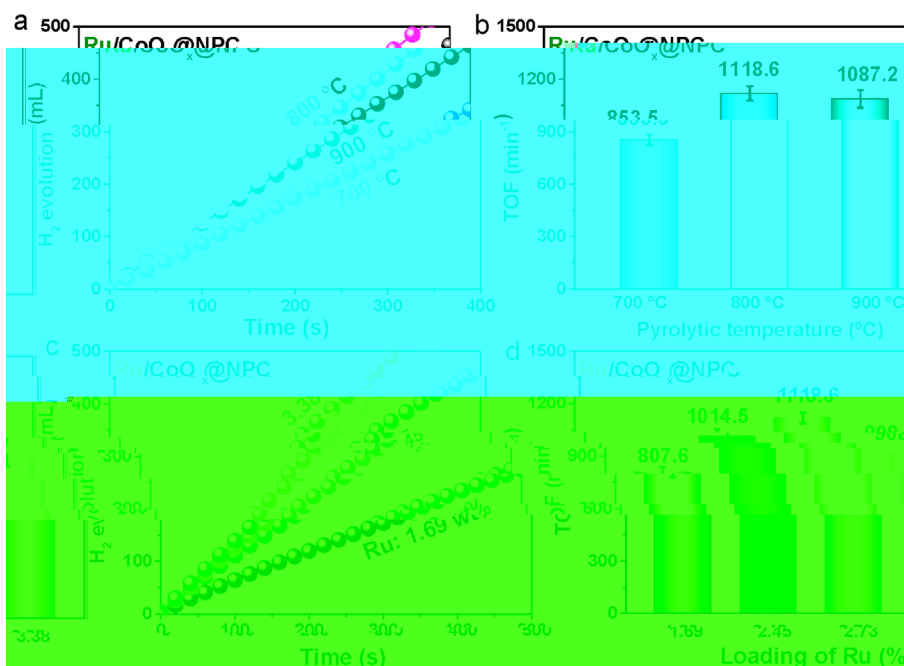


Fig. 4 – (a) Stoichiometric H₂ evolution and (b) the summarized TOF values by Ru/CoO_x@NPC catalysts with different pyrolysis temperatures at 25 °C. (c) The relationship between the H₂ generation rates and loadings of Ru species on Ru/CoO_x@NPC catalysts, and (d) the summarized TOF values. All the experiments are conducted in 150 mM NaBH₄ + 0.4 wt % NaOH solution at 25 °C.

loaded powder catalyst for NaBH_4 hydrolysis (Table S4) of the above knowledge. In addition, the optimal loading of Ru in the morphology of catalysts. The results show that the concentration of Ru increases, the catalytic hydrogen generation increases rapidly from the beginning and then slowly down when it reaches the maximum point around 3.0% (Fig. 4c). The catalyst has the large TOF value when the Ru loading is 2.73% (Fig. 4d). The results showed that the Ru/CoO@NPC prepared by the precipitation of Co/Zn ratio of 3/4 has the best catalytic performance (Fig. S8). The equivalent H_2 per mole of NaBH_4 added in the electrocatalytic reaction changes in concentration (Fig. S9a–b). Therefore, the Ru loading in the Ru/CoO@NPC catalyst decreased below 2.73%, and CoO@NPC is prepared by cobalt ion at 800 °C in ammonia.

To evaluate the effect of different supports on the catalytic performance, we investigated the catalytic performance on various supports with the same loading of Ru (2.73%). As shown in Fig. 5a and Fig. S9c, the catalytic activity of Ru loaded CoO@NPC is found to be the highest than that of CoO@NPC, all other catalysts. Fig. 5b shows that the HGR value of Ru/CoO@NPC is 8019.5 $\text{mL min}^{-1} \text{g}^{-1}$ (total mass of catalyst), which is 1.44–, 4.57–, 716.0– and 47.53–fold higher than that of Ru/CoO@NC-67, Ru/CB, Ru/NPC-8 and NPC-67 respectively, while all other supports of the previous reported catalysts (Table S4). In particular, the metal ICP-AES results show that the concentration of Zn in the catalyst is 1% and 3%. In combination with Fig. 5a, the catalytic performance of Ru/NPC-8 is weak, indicating that Zn has a little effect on the performance of catalytic hydrogen evolution as an impurity. To measure the activation energy of

Ru/CoO@NPC and Ru/CoO@NC-67, a series of experiments were conducted at different temperatures. As shown in Fig. 5c and Fig. S9d, the rate of HGR also increases rapidly with increasing the reaction temperature from 298 K to 318 K, and the rate constant k is calculated from the slope of each experiment. The activation energy of Ru/CoO@NPC catalyst was estimated to be 54.2 kJ mol^{-1} by the Arrhenius plot ($\ln k$ vs $1/T$), which is lower than that of Ru/CoO@NPC (59.3 kJ mol^{-1}) (Fig. 5d and Fig. S10), implying a kinetically enhanced catalytic activity of NaBH_4 hydrolysis [51].

Due to the advantages of the stability of Ru/CoO@NPC catalyst in an alkaline NaBH_4 solution (Fig. 6a). The results show that the Ru/CoO@NPC catalyst exhibits excellent stability for catalytic hydrogen generation. After the first cycle, it retained ca. 73.9% of initial activity (Fig. 6b). The high decay of catalytic activity could be attributed to the desorption of Ru species (the mass fraction of Ru species increased from 2.73% to 2.10% by ICP-AES after the first cycle, Table S3), catalyst damage (Fig. S11) and catalyst poisoning by BO_2^- species [28,52].

As discussed above, the Ru/NPC@CoO catalyst has the large HGR and TOF value as compared to the catalyst. The outstanding performance mainly attributed to the large specific surface area, high conductivity, and negative charge of Ru species. According to the XPS data, the positive shift of the Co 2p binding energy in Ru/CoO@NPC catalyst by the partial electron transfer from Co species to Ru species indicates a higher electron density on Co species as compared to that of Ru species. Accordingly, the partial negative charge of hydrogen atom preferred to adsorb the Ru atom. As a result, the BH_4^- dissociates at the Co and Ru metal sites, on which hydrogen atom adsorbed on Ru and BH_3 is

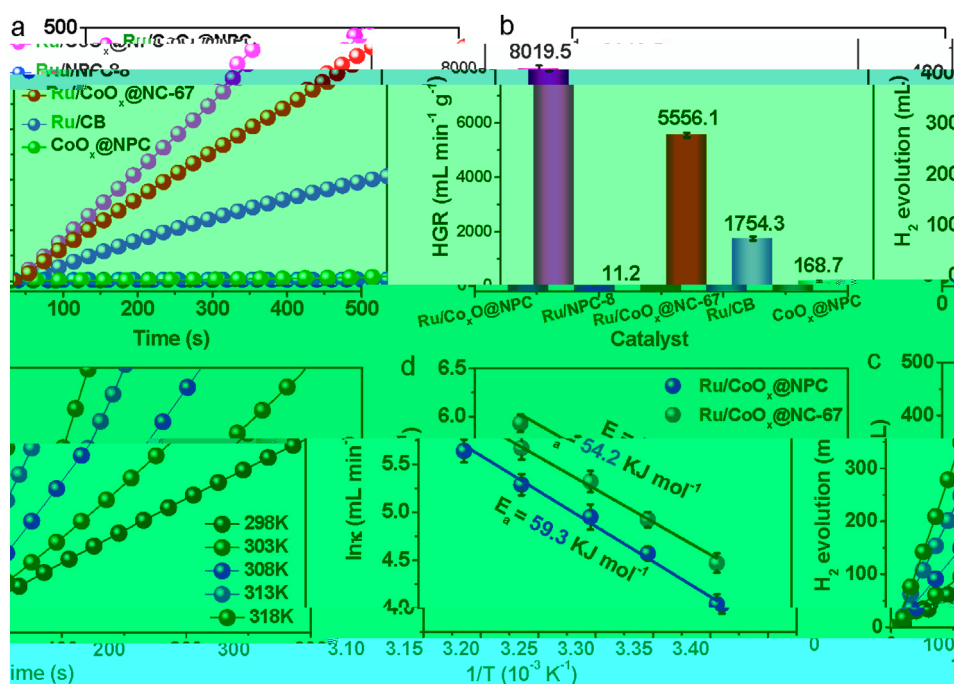


Fig. 5 – (a) Stoichiometric H_2 evolution and (b) the summarized TOF values of different catalysts (2.73 wt% Ru) in 150 mM NaBH_4 + 0.4 wt% NaOH solution at 25 °C. (c) Stoichiometric H_2 evolution of Ru/CoO_x@NPC in 150 mM NaBH_4 + 0.4 wt% NaOH solution at different reaction temperatures, and (d) the summarized Arrhenius plots from c.

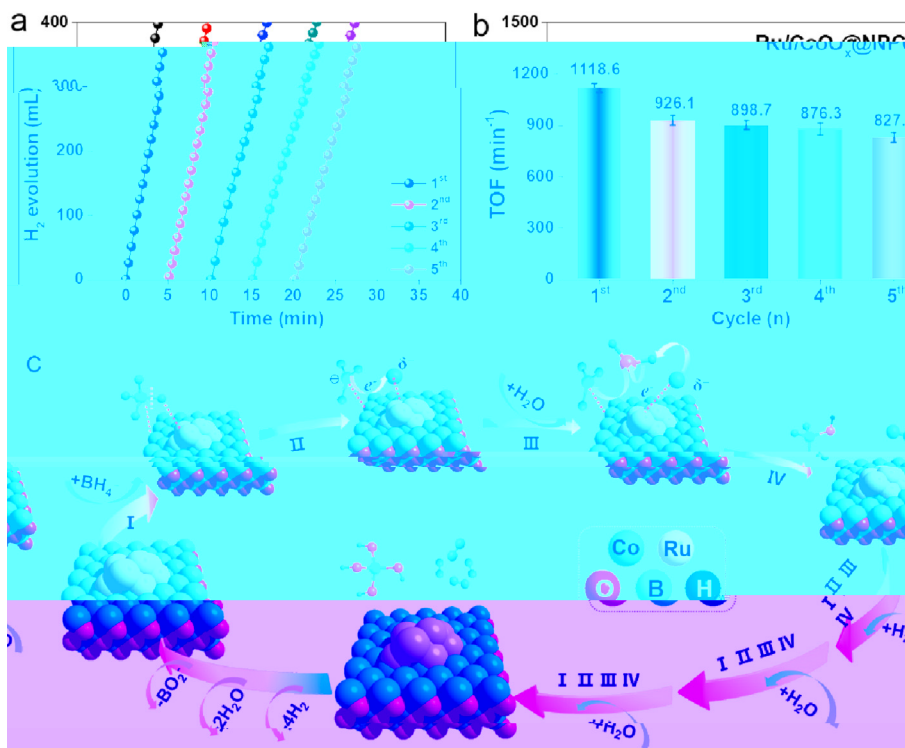


Fig. 6 – (a) Reusability test of Ru/CoO_x@NPC catalyst in 150 mM NaBH₄ + 0.4 wt % NaOH at 25 °C. (b) The summarized TOF values in different reusability test. (c) The proposed catalytic mechanism of Ru/CoO_x@NPC catalyst for H₂ generation.

attached to Co species. After the B–H bond is broken, the negatively charged B species immediately transfers the negative charge to the adsorbed H atom, although the conductivity is low. Finally, the negatively charged H atom on the Ru surface reacts with H₂ to form a BH₃OH molecule, while the OH⁻ ion attacks the BH₃ to form a BH₃OH molecule, followed by the formation of the BH₃OH intermediate. After the cycle, the surface of the catalyst is regenerated by the adsorption of BH₃OH species. As the reaction proceeds, all of the H atoms in the borohydride are replaced by OH⁻ ions (Fig. 6c), limiting the release of the B(OH)₄⁻ species [53].

Conclusion

In this work, we synthesized ZIF-8@ZIF-67 catalyst, which is a highly porous material composed of ZIF-8 and ZIF-67, a well-established and fabricated using a seed-mediated growth technique. Upon the direct combination of ZIF-8@ZIF-67 catalyst, a novel CoO@NPC porous catalyst was generated. The functionalized porous structure has a high surface area (325.0 m² g⁻¹) derived from ZIF-8 and porous morphology inherited from ZIF-67. Finally, the low loading of Ru decorated CoO@NPC catalyst showed high chemical stability. The combination of porous structure, porous morphology, and loading concentration of Ru chloride resulted in the optimal performance on NaBH₄ hydrolysis, which achieved the best condition for the hydrolysis at 800 °C,

and the Ru loading is 2.37%. The high TOF value of Ru/CoO@NPC catalyst is 1118.6 min⁻¹ at 25 °C, far better than most reported catalysts. Besides, the Ru/CoO@NPC catalyst still maintains more than 70% catalytic activity after five cycles. This work provides a new insight into designing and preparing a highly active catalyst for NaBH₄ hydrolysis.

Declaration of competing interest

The authors declare that they have no known competing financial interests or personal relationships that could have appeared to influence the work reported in this paper.

Acknowledgements

This work has been supported by the National Natural Science Foundation of China (no. 21965005), National Science Foundation of Guangxi Province (2018GXNSFAA294077, 2018GXNSFAA281220), Project of High-Level Talents of Guangxi (F-KA18015, 2018ZD004) and Guangxi Technology Base and Talents Project (GUIKE AD18126001).

Appendix A. Supplementary data

Supplementary data associated with this article can be found online at <http://doi.org/10.1016/j.ijhydene.2020.12.011>.

REFERENCES

- [1] L XF, Y L, Lo XW. High efficiency Ni-doped FeP/carbon hollow nano-rod as a pH-efficient and durable hydrogen evolution electrocatalyst. *Sci. Adv.* 2019;5:eaa6009.
- [2] Huang LB, Zhao L, Zhang Y, Chen YY, Zhang QH, Luo H, Zhang X, Tang T, Guo L, Han JS. Self-limited one-pot synthesis of MoO₃ nanorods in one-pot aligned layered MoS₂ monolayer MoS₂ for efficient hydrogen evolution. *Adv. Energy Mater.* 2018;8:1800734.
- [3] Tang C, Zhang R, Liu W, He L, Jiang X, Ai AM, Sun X. Fe-doped CoP nanorods: a monolithic multifunctional catalyst for high-efficiency hydrogen evolution. *Adv. Mater.* 2017;29:1602441.
- [4] Ghodke NP, Rapal S, Bhojka SV, Mahesh VL. Catalytic hydrogen evolution from water using nickel nanorods. *J. Hydrogen Energy* 2020;45:16591–605.
- [5] Ebele U, Miller B, Helmolt R. Fuel cell electrocatalysis and hydrogen evolution: a review. *Energy Environ. Sci.* 2012;5:8780–98.
- [6] Schneemann A, White JL, Kang S, Jeong S, Wan LF, Cho ES, Heo TW, Pendergast D, Urban JJ, Wood BC, Allendoerfer MD, Saito V. Nanostructured metal hydride for hydrogen storage. *Chem. Rev.* 2018;118:10775–839.
- [7] Aakko-Sak PT, Cook C, Kiah J, Repo T. Liquid organic hydrogen carrier for transport and storage of renewable energy – electrolysis and discharge. *J. Power Sources* 2018;396:803–23.
- [8] Yao Q, Li Z-H, Huang W, Chen X, Zhang J. High P-like activity of the Ni–Mo/glycophane catalyst for hydrogen evolution from hydrogen evolution of ammonia borane. *J. Mater. Chem. A* 2016;4:8579–83.
- [9] Mori K, Miyazaki K, Yamahira H. Rhenium- and Rhodium-nanoparticle on TiO₂ for photoelectrochemical hydrogen production from ammonia-borane. *ACS Catal.* 2016;6:3128–35.
- [10] Yan H, Heo W, Hao Y, Wang Y, Qiao W, Wang T, Zhang X. Hydrogen evolution from hydrogen evolution of ammonia borane using nanostructured NiB amorphous catalyst. *Nano* 2020;15:2050081.
- [11] Urdakan A, Demir Y. Hydrogen evolution from ammonia borane for hydrogen evolution from ammonia-borane. *J. Hydrogen Energy* 2019;44:17586–94.
- [12] Zhang Y, Ouyang L, Zhong H, Li J, Wang H, Shao H, Huang Z, Zhang M. Constructing the loop for hydrogen evolution: facile synthesis of Ni-B nanorods for efficient hydrogen evolution. *Angew. Chem. Int. Ed.* 2020;59:8623–9.
- [13] Ouyang L, Chen W, Li J, Feldehoff M, Wang H, Zhang M. Enhancing the hydrogen evolution rate of Ni-B nanorods for hydrogen evolution. *Adv. Energy Mater.* 2017;7:1700299.
- [14] Zhang X, Zhang Q, Xu B, Li X, Zhang K, Fan G, Jiang W. Efficient hydrogen evolution from Ni-B nanorods for hydrogen evolution. *ACS Appl. Mater. Interfaces* 2020;12:9376–86.
- [15] Zhong H, Ouyang L, Zeng M, Li J, Wang H, Shao H, Feldehoff M, Zhang M. Realizing facile hydrogen evolution of Ni-B nanorods for hydrogen evolution. *J. Mater. Chem. A* 2019;7:10723–8.
- [16] Li J, Wang H, Yan Q, Song X. A novel metal-organic framework for hydrogen evolution. *J. Power Sources* 2018;395:8–15.
- [17] Abdelhamid HN. Hierarchical porous ZIF-8 for hydrogen evolution. *Dalton Trans.* 2020;49:4416–24.
- [18] Wang C, Zhang J, Guo J, Sun L, Ming J, Dong H, Zhao Y, Tian J, Yang X. Ceia-induced aegonite-like porous cobalt-nickel oxide and heterogeneous effective hydrogen evolution. *ACS Sustainable Chem Eng* 2018;6:7451–7.
- [19] Zhang H, Zhang L, Rodriguez-Pérez IA, Miao W, Chen K, Wang W, Li Y, Han S. Carbon nanoporous electrode for bismuth-like P-Co alloy catalyst for NaBH₄ hydrogen evolution. *Appl. Sci.* 2021;540:148296.
- [20] Wang C, Guo J, Zhang J, Zhao Y, Tian J, Imamjan TT, Yang X. Palladium nanorods decorated porous ZIF-67 polyhedron for high catalytic activity and stability for hydrogen evolution. *Renew. Energy* 2019;136:1064–70.
- [21] Al-Thabai SA, Khan Z, Malik MA. Bismuth-like Ag-Ni nanoparticles as an efficient catalyst for hydrogen evolution from hydrogen evolution of ammonia borane. *J. Hydrogen Energy* 2019;44:16452–66.
- [22] Ruff S, Sauer AM V. Carbon porous electrode bismuth-like Rhenium-Co catalyst for hydrogen evolution from ammonia borane. *J. Energy Res.* 2018;42:1183–95.
- [23] Tian DD, Lin K-YA. Rhenium porous electrode on ZIF-67 as an enhanced catalyst for hydrogen evolution from ammonia borane. *Chem. Eng. J.* 2018;351:48–55.
- [24] Wei Y, Wang M, Fan W, Wei L, Zhao X, Zhou X, Ni M, Wang H. High activity and durable catalyst for hydrogen evolution from ammonia borane. *Chem. Commun.* 2020;836:155429.
- [25] Kim C, Lee SS, Li W, Fong JD. Top-down synthesis of cobalt-based metal-organic nanocatalyst for hydrogen evolution from ammonia borane. *Appl. Catal. A Gen.* 2020;589:117303.
- [26] Akdim O, Demirci UB, Miele P. Deactivation and reactivation of cobalt in hydrogen evolution of ammonia borane. *J. Hydrogen Energy* 2011;36:13669–75.
- [27] Xu J, Dong X, Wei Q, Huang Y. Efficient hydrogen evolution from ammonia borane on Ni-B porous electrode. *Chem. Commun.* 2020;5:6683–90.
- [28] Guo J, Wang C, Zhang J, Yan P, Tian J, Shen X, Imamjan TT, Yang X. Hierarchical porous cobalt-like Rhenium-CoP as a catalyst for hydrogen evolution. *J. Mater. Chem. A* 2019;7:8865–72.
- [29] Pan Y, Sun K, Li S, Cao X, Wang K, Cheng WC, Chen Z, Wang Y, Li Y, Li Y, Wang D, Peng Q, Chen C, Li Y. Coe-hell ZIF-8@ pf-67-derived CoP nanoparticle-embedded N-doped carbon nanorods for efficient hydrogen evolution. *J. Am. Chem. Soc.* 2018;140:2610–8.
- [30] Tang J, Salnikhe RR, Li J, Toad NL, Imamjan M, Fan W, Yamachi Y. The metal-organic framework of cobalt-organic framework: a new method for electrocatalytic hydrogen evolution. *J. Am. Chem. Soc.* 2015;137:1572–80.
- [31] Deng LYD, Chen X, Wang G, Jin L, Pan X, Deng J, Sun G, Bao X. Ion encapsulated hydrogen evolution-like carbon nanorods for hydrogen evolution. *Angew. Chem., Int. Ed.* 2013;52:371.
- [32] Guo RSD, Akiba C, Saji S, Kondo T, Nakamura J. Activity of nickel-doped carbon material for hydrogen evolution. *Science* 2016;351:361.
- [33] Cui L, Xu Y, Ni L, Yang W, Li J. Multifunctional inorganic CoP nanorods as an on/off switch for efficient on-demand hydrogen evolution from ammonia borane and NH₃BH₃. *Nano Res.* 2017;10:595–604.
- [34] Yao Q, Li Z-H, Yang Y, Chen Y, Chen X, Jiang H-L. Facile synthesis of glycophane-porous Ni-CeO₂ nanocomposite as a high-efficiency catalyst for hydrogen evolution from ammonia borane. *Nano Res.* 2018;11:4412–22.
- [35] Wang Z, Li Y, Yan Y, Liang TYP, Zhang X, Wang D, Zhang H, Yang Y, Wang X. Coe-hell carbon material derived from

- metal-organic framework as an efficient oxygen bifunctional electrocatalyst. *Nano Energy* 2016;30:368–78.
- [36] Li S, Wang Z, Zhou S, Yang F, Yang M, Chiang C-Y, Zhou W, Zhao J, Qi J. Metal-organic-framework-derived bifunctional electrocatalyst for oxygen reduction and evolution. *Adv Mater* 2017;29:1700874.
- [37] Tang C, Sunkara A-E, Chen F, Pohl M-M, Agostini G, Schneide M, Jung H, Belle M. A stable nano-cobalt catalytic electrode for oxygen reduction of formic acid in highly dispersed CoN acrylate. *Angew Chem Int Ed* 2017;56:16616–20.
- [38] Joo SH, Park JY, Ren J, Borch DR, Han W, Somjai GA. Site effect of hemimorphite in catalytic carbon monoxide oxidation. *Nano Lett* 2010;10:2709–13.
- [39] Ma X, Zhao X, Han J, Sun L, Li Q, Yang X. Fine Carbon nanotube encapsulated in a N-doped porous carbon matrix for special N-doped porous carbon nanobelt for efficient oxygen reduction. *ACS Appl Mater Interfaces* 2017;9:21747–55.
- [40] Tong Y, Chen P, Zhou T, Xu K, Chen W, Wang C, Xie Y. A bifunctional hybrid electrocatalyst for oxygen reduction and evolution: cobalt oxide nanotubes on graphitic carbon nitride. *Angew Chem Int Ed* 2017;56:1–6.
- [41] Li Y, Zhang LA, Qin Y, Chen F, Kong Y, Tao Y, Li Y, Bai Y, Ding D, Li M. Cation dependence of hemimorphite nanocatalyst for hydrogen evolution reaction. *ACS Catal* 2018;8:5714–20.
- [42] Yang X, Wang X, Feng Y, Zhang G, Wang T, Song W, Shao C, Jiang L, Wang C. Removal of multifold hexagonal conformation in doped layered porous magnetic Fe₂O₃@Al(OH)₃ for electrocatalysis. *J Mater Chem A* 2013;1:473–7.
- [43] Guo J, Wang B, Yang D, Wan Z, Yan P, Tian J, Iimjan TT, Yang X. RGO-like Ni₂P-CoP nanosheets as a bifunctional electrocatalyst for hydrogen evolution: NaBH₄ hydride and electrocatalysis. *Appl Catal B: Environ* 2020;265:118584.
- [44] Qian M, Xu M, Zhou S, Tian J, Talat Iimjan T, Shi Z, Yang X. Template synthesis of two-dimensional layered nickel-cobalt-nitrogen co-doped porous carbon film: promoting the conductivity and electrocatalytic performance. *J Colloid Interface Sci* 2020;564:276–85.
- [45] Noio F, Filippo K, Chaudhry B. Location and dynamics of CO adsorption on Ru nanoparticles: a solid-state NMR study. *Chem Lett* 2010;140:1–7.
- [46] Zhang R, Li Y, Wei L, Fang Z, Li C, Ni Y, Xu Z, Tao S, Li P. Synthesis of a porous carbon nanotube network for efficient electrocatalysis. *Appl Catal B: Environ* 2017;191:119–27.